

COMPUTATIONAL EFFICIENCY AND QUALITY OF DIFFERENT VERSIONS OF DISCONTINUOUS GALERKIN METHOD FOR LES/DES APPLICATIONS

I. Bosnyakov*, A. Troshin*, V. Vlasenko*, A. Wolkov*
*Central Aerohydrodynamic Institute (TsAGI)

Keywords: *discontinuous Galerkin, dual time stepping, large eddy simulation*

Abstract

Dual time stepping (DTS) time integration techniques for Discontinuous Galerkin (DG) method are presented for one-dimensional Burgers equation and for full three-dimensional Navier–Stokes equation system. Unfiltered and spatially filtered equations with Smagorinsky subgrid scale model are considered which are compared in terms of energy spectrum resolution capability. Presented time integration techniques are applicable to unsteady large eddy simulation problems and are designed to be unconditionally stable in viscous regions of the flow. Computational efficiency of different (1–4) temporal order DTS techniques is compared to the efficiency of the explicit DG scheme in two test cases. All computations are performed with constant global physical time step. High order spatial and temporal discretizations as well as implicit first order pseudo-time scheme are described in details.

1 Overview of equations and their approximation

Both one-dimensional Burgers equation and three-dimensional Navier–Stokes equation system one can be represented in the following form:

$$\frac{\partial \mathbf{U}}{\partial t} + \nabla \cdot \mathbf{F}(\mathbf{U}, \mathbf{G}) = 0.$$

\mathbf{U} is vector of conservative variables, \mathbf{G} consists of spatial \mathbf{U} derivatives (gradients),

and \mathbf{F} are the fluxes of \mathbf{U} . It is convenient to represent fluxes as a sum of convection and diffusion contributions: $\mathbf{F} = \mathbf{F}^{\text{conv}} + \mathbf{F}^{\text{diff}}$. Diffusive fluxes consist of molecular and subgrid parts.

1.1 One-dimensional Burgers equation

This equation can be considered as a simplification of Navier–Stokes equation system. There is one variable u , so $\mathbf{U} = u$. Convective flux is actually a scalar, it is nonlinear and defined as $F^{\text{conv}} = u^2 / 2$. Diffusive flux is

$$F^{\text{diff}} = - \left(\mu + C_s h^2 \left| \frac{\partial u}{\partial x} \right| \right) \frac{\partial u}{\partial x}.$$

When no spatial filtering is applied, $C_s = 0$ (hereinafter, this version of equation is called “ILES”, which refers to Implicit LES [1]). With spatial filtering, we use $C_s = 0.2$ by default which corresponds to Smagorinsky subgrid scale model for Burgers equation (with subgrid viscosity coefficient μ_{SGS} defined as $h^2 |\partial u / \partial x|$). We designate the filtered version of equation as “LES”. Here h is cell size.

To sum up, we consider one-dimensional Burgers equation of the form

$$\frac{\partial u}{\partial t} + \frac{\partial}{\partial x} \left[\frac{u^2}{2} - \left(\mu + C_s h^2 \left| \frac{\partial u}{\partial x} \right| \right) \frac{\partial u}{\partial x} \right] = 0.$$

1.2 Three-dimensional Navier–Stokes equation system

In case of Navier–Stokes equation system, \mathbf{U} is $[\rho; \rho u; \rho v; \rho w; \rho E]^T$.

Vectors of convective fluxes along axes:

$$\mathbf{F}_x^{\text{conv}} = \begin{bmatrix} \rho u \\ \rho u^2 + p \\ \rho uv \\ \rho uw \\ \rho uH \end{bmatrix} \quad \mathbf{F}_y^{\text{conv}} = \begin{bmatrix} \rho v \\ \rho uv \\ \rho v^2 + p \\ \rho vw \\ \rho vH \end{bmatrix} \quad \mathbf{F}_z^{\text{conv}} = \begin{bmatrix} \rho w \\ \rho uw \\ \rho vw \\ \rho w^2 + p \\ \rho wH \end{bmatrix}$$

Vectors of diffusive fluxes along axis i :

$$\mathbf{F}_i^{\text{diff}} = \begin{bmatrix} 0 \\ \tau_{xi} \\ \tau_{yi} \\ \tau_{zi} \\ \tau_{xi} u + \tau_{yi} v + \tau_{zi} w + \sigma_i \end{bmatrix}.$$

Closing relations for Navier–Stokes equation system are state equation $p = \rho RT$, expressions for total energy and enthalpy of gas mass unit

$$E = \frac{u^2 + v^2 + w^2}{2} + \frac{RT}{\gamma - 1},$$

$$H = \frac{u^2 + v^2 + w^2}{2} + \frac{\gamma RT}{\gamma - 1}, \quad \gamma = 1.4,$$

expression for dynamic coefficient of molecular viscosity

$$\mu = 1.72 \cdot 10^{-5} \cdot \left(\frac{T}{273} \right)^{3/2} \frac{273 + 122}{T + 122} \frac{\text{kg}}{\text{m} \cdot \text{s}},$$

expressions for tensor components of momentum diffusive and subgrid fluxes

$$\tau_{ij} = -(\mu + \mu_{SGS}) \left(2S_{ij} - \frac{2}{3} \text{div} \mathbf{V} \delta_{ij} \right),$$

$$S_{ij} = \frac{1}{2} \left(\frac{\partial u_i}{\partial x_j} + \frac{\partial u_j}{\partial x_i} \right),$$

expressions for vector components of heat energy diffusive fluxes

$$\sigma_i = - \left(\frac{\mu}{\text{Pr}} + \frac{\mu_{SGS}}{\text{Pr}_T} \right) C_p \frac{\partial T}{\partial x_i}, \quad C_p = \frac{\gamma R}{\gamma - 1},$$

$$\text{Pr} = 0.72, \quad \text{Pr}_T = 0.9,$$

subgrid scale viscosity coefficient formula [2]

$$\mu_{SGS} = \rho (C_s \Delta)^2 \sqrt{2S_{ij}S_{ij}}, \quad \Delta = \sqrt[3]{V_\Omega},$$

where V_Ω is cell volume.

1.3 DG method equation system

DG solution in each point is represented as a linear combination of local polynomial basis functions $\varphi_j(\mathbf{x})$:

$$\mathbf{U} = \sum_{j=1}^{K_f} \mathbf{u}_j \varphi_j(\mathbf{x}).$$

Equation system is multiplied by basis function $\varphi_i(\mathbf{x})$ and integrated over the cell volume Ω . After integration by parts and applying Gauss–Ostrogradsky formula, the following equation is obtained:

$$\int_{\Omega} \frac{\partial \mathbf{U}}{\partial t} \varphi_i(\mathbf{x}) d\Omega + \int_{\Sigma} (\mathbf{F} \cdot \mathbf{n}) \varphi_i(\mathbf{x}) d\Sigma = \int_{\Omega} (\mathbf{F} \cdot \nabla \varphi_i(\mathbf{x})) d\Omega. \quad (1)$$

Dual time stepping time discretization [3] requires finite difference approximation of unsteady term which is $(\partial \mathbf{U} / \partial t)^{n+1} \approx$

$$\frac{\mathbf{U}^{n+1} - \mathbf{U}^n}{\tau} \quad (1 \text{ order}),$$

$$\frac{3\mathbf{U}^{n+1} - 4\mathbf{U}^n + \mathbf{U}^{n-1}}{2\tau} \quad (2 \text{ order}),$$

$$\frac{11\mathbf{U}^{n+1} - 18\mathbf{U}^n + 9\mathbf{U}^{n-1} - 2\mathbf{U}^{n-2}}{6\tau} \quad (3 \text{ order}),$$

$$\frac{25\mathbf{U}^{n+1} - 48\mathbf{U}^n + 36\mathbf{U}^{n-1} - 16\mathbf{U}^{n-2} + 3\mathbf{U}^{n-3}}{12\tau} \quad (4 \text{ order}),$$

or in general form,

$$\left(\frac{\partial \mathbf{U}}{\partial t} \right)^{n+1} \approx \frac{1}{\tau} \left[\gamma_* \mathbf{U}^{n+1} + \sum_k \gamma_k \mathbf{U}^{n-k} \right].$$

Substituting this formula into (1) and introducing pseudo-time ξ , we obtain

$$\begin{aligned} & \int_{\Omega} \frac{\partial U}{\partial \xi}(\xi) \varphi_i(\mathbf{x}) d\Omega + \\ & \frac{1}{\tau} \int_{\Omega} (\gamma_* U(\xi) + \sum_k \gamma_k U^{n-k}) \varphi_i(\mathbf{x}) d\Omega + \quad (2) \\ & \oint_{\Sigma} (\mathbf{F}(\xi) \cdot \mathbf{n}) \varphi_i(\mathbf{x}) d\Sigma = \int_{\Omega} (\mathbf{F}(\xi) \cdot \nabla \varphi_i(\mathbf{x})) d\Omega. \end{aligned}$$

At the initial pseudo-time moment $\xi = \xi^{(0)}$, we take $U(\xi^{(0)}) = U^n$, and solve the equation system (2) till the moment when a stationary state in pseudo-time is reached, i.e. until $\partial U / \partial \xi = 0$. At that moment, the first term in (2) disappears, and (2) coincides with (1) (with $U(\xi)$ replaced by U^{n+1}). If the stationary state is unique, it will coincide with U^{n+1} , i.e. we get the solution of the system (1) at unknown physical time layer t^{n+1} . A simple choice for pseudo-time marching is one-step backward Euler implicit scheme.

Other features of the particular DG implementation are: orthonormal polynomial basis function set [4], Riemann solver by Roe, BR2 viscous terms approximation [5], Gauss-Seidel linear equation system solver [6]. The details of our earlier DG implementation can be found in [7].

2 One-dimensional Burgers turbulence test

2.1 Computational domain, initial and boundary conditions

A one-dimensional computational domain $[-L, L]$ with periodic boundary conditions is used in this test. Initially, a random spatially uncorrelated field $u(x, 0)$ is generated with Gaussian distribution.

The distribution is centered: $\langle u(x, 0) \rangle = 0$ and has average amplitude $\langle u^2(x, 0) \rangle^{1/2} = 10$. It is allowed to evolve in a highly resolved numerical computation on a dense mesh using high order explicit DG scheme up to the moment when $\langle u^2(x, t) \rangle^{1/2} = 1$. At this moment,

a typical Burgers turbulence forms (Fig. 1) with clear $E(\kappa) \sim \kappa^{-2}$ energy spectrum region (Fig. 2). Here

$$\begin{aligned} E(\kappa) &= \frac{U_r^2(\kappa) + U_i^2(\kappa)}{2}, \\ U_r &= \int_{-L}^L \frac{u(x) \cos \kappa x}{2\pi} dx, \quad U_i = \int_{-L}^L \frac{u(x) \sin \kappa x}{-2\pi} dx. \end{aligned}$$

In this computation, low viscosity coefficient value $\nu = 10^{-4}$ is used. Resulting field is considered initial for further computations.

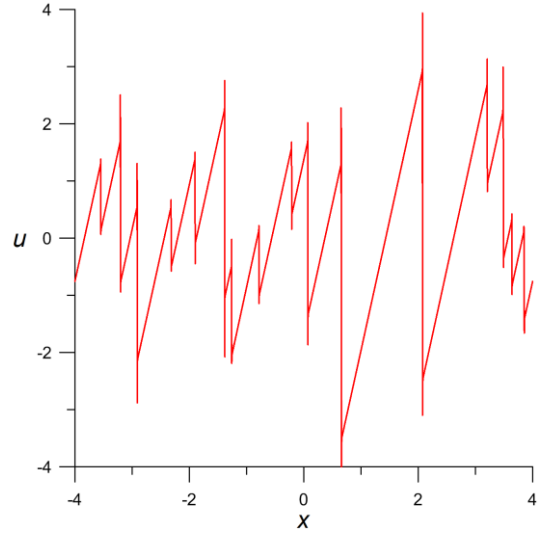


Fig. 1. Burgers turbulence as a result of initial random field evolution in time

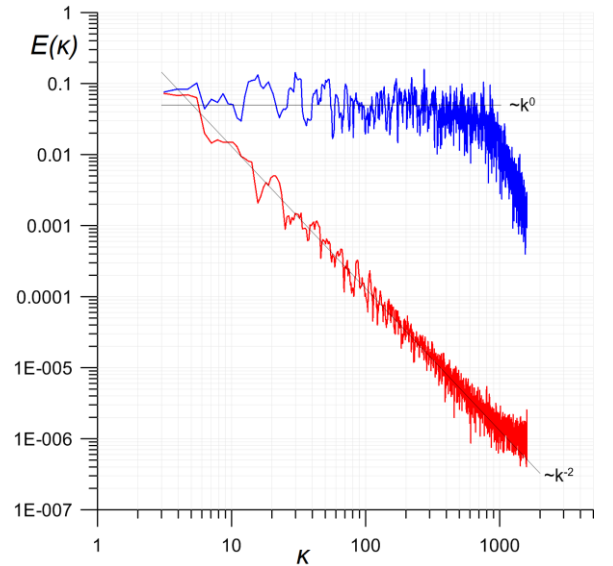


Fig. 2. Energy spectra of initial uncorrelated field (blue) and Burgers turbulence (red)

2.2 Computational meshes, models, and numerical scheme settings

Three types of computations were conducted, representing “Direct numerical simulation” (“DNS”), “Implicit large eddy simulation” (“ILES”), and “Large eddy simulation” (“LES”). Viscosity coefficient ν was taken to be 10^{-3} .

In all computations, DG method was used with quadrature rules that provide exact integrals for the polynomials used, i.e. $K+1$ Gauss points inside each 1D element for K^{th} order basis functions.

“DNS” computations were performed on a mesh with 2048 cells with DG $K=3$ and $K=6$ using global time stepping ($\text{CFL} = 10^{-2}$, where $\text{CFL} = \Delta t \max\{|u|\}/h$). The differences between $K=3$ and $K=6$ were found to be negligible (energy spectra differ at wavenumbers $\kappa > 1200$) which indicates polynomial convergence of the solution.

“ILES” computations were performed on a mesh with 128 cells with DG $K=1$ (256 DOFs). Both explicit global time stepping and 1–4 order DTS (hereinafter denoted as DTS1, DTS2, DTS3, and DTS4) with physical CFL = 2, 1, 0.5, 0.1 were used.

“LES” computations were performed on a mesh with 64 cells with DG $K=3$ (the same NDOFs as in “ILES”). As with “ILES”, explicit global time stepping and DTS1–DTS4 were used.

2.3 Results processing

All computations were run until turbulent kinetic energy

$$k = \int_{-L}^L \frac{u^2}{2} dx$$

equals $k_0/20$, where k_0 is its initial value. Turbulent kinetic energy is integrated over the whole computational region using the same Gauss quadrature rules as in the rest of the numerical scheme. $k(t)$ dependence on an interval from $k_0/2$ to $k_0/20$ is extracted and compared between computations.

Energy spectrum $E(\kappa)$ at the final moment of computation is determined and compared; spectrum is obtained using wavenumbers $\kappa = N_i \frac{2\pi}{L}$, where $N_i = 2, 4, \dots, N_{\text{cells}}$ (N_{cells} is the number of cells in the computational mesh). Integration is done over all cells; each cell is divided uniformly by 10 points with equal weights.

2.4 Reference solution

$k(t)/k_0$ plots obtained in “DNS” computations are shown on Fig. 3. Red dashed line corresponds to $K=3$, blue dashed line corresponds to $K=6$. Evidently, lines coincide. $E(\kappa)$ plot at the final moment of time is shown on Fig. 4. A clear κ^{-2} spectrum is obtained for $\kappa \leq 100$ followed by viscous damping region.

2.5 Solutions comparison in terms of accuracy

At first, solution accuracy was compared in explicit global time stepping computations with $\text{CFL} = 10^{-3}$ to eliminate influence of temporal discretization on the results. In Fig. 5 and 6, $k(t)/k_0$ and $E(\kappa)$ plots are compared between “DNS”, “ILES”, and “LES”.

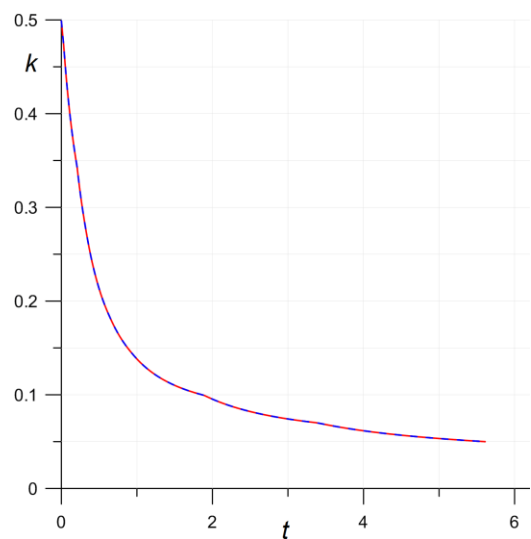


Fig. 3. Turbulent kinetic energy decay $k(t)/k_0$ in reference computation. Red dashed line – $K=3$, blue dashed line – $K=6$

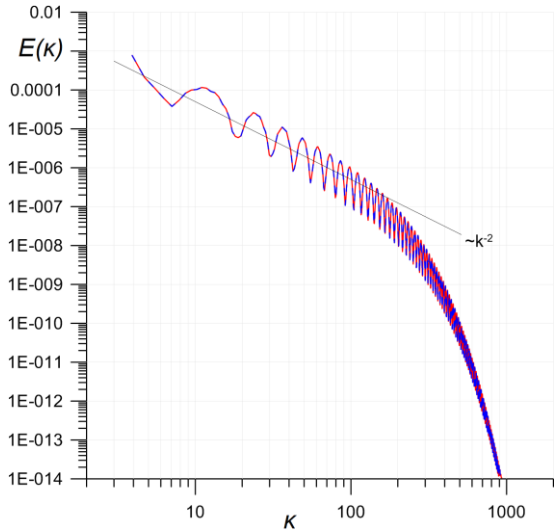


Fig. 4. Energy spectra $E(\kappa)$ in reference computation. Lines as in Fig. 3.

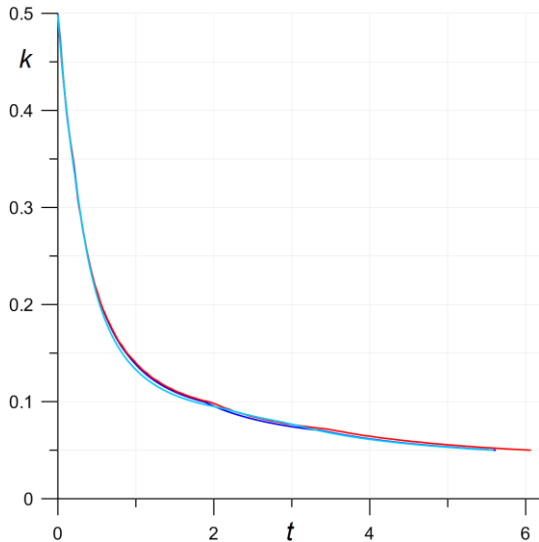


Fig. 5. Turbulent kinetic energy decay $k(t)/k_0$. Lines: blue – “DNS”, red – “ILES” $K = 1$, light-blue – “LES” $K = 3$

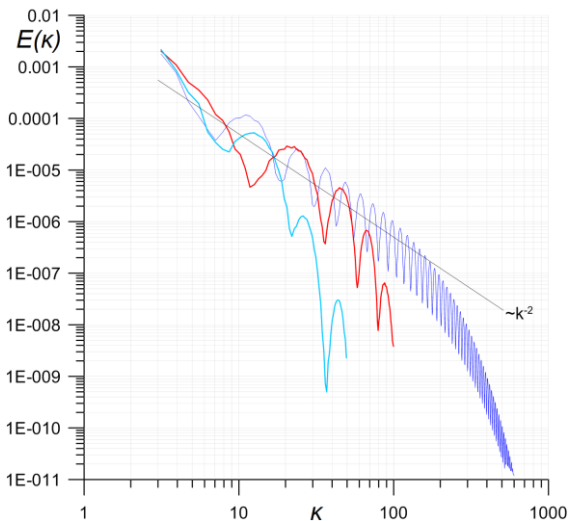


Fig. 6. Energy spectra $E(\kappa)$. Lines as in Fig. 5.

All models give approximately the same $k(t)$ dependence which indicates that energy is transferred from large scales to small. In other words, small scale motions do not influence the dynamics of large scale energy containing motions. This justifies the use of ILES technique: depending on the numerical scheme, small scale motions may be simulated incorrectly, but this does not spoil large scale turbulence which is of engineering importance. This result is true at least for Burgers equation.

Concerning the spectrum, in $K = 3$ “LES” solution with Smagorinsky subscale model and $C_s = 0.2$, the spectrum is highly damped in $\kappa > 20$ region. In $K = 1$ “ILES” solution, the κ^{-2} spectrum is resolved up to $\kappa = 50$. This result suggests trying Smagorinsky subgrid model with lower C_s or even $K = 3$ “ILES” in the future.

After that, DTS influence was studied in a series of DTS1–DTS4 computations. The resulting $k(t)/k_0$ and $E(\kappa)$ plots for initial CFL = 2 are shown in Fig. 7–10. During the computation, CFL drops approximately 5 times relative to its initial value.

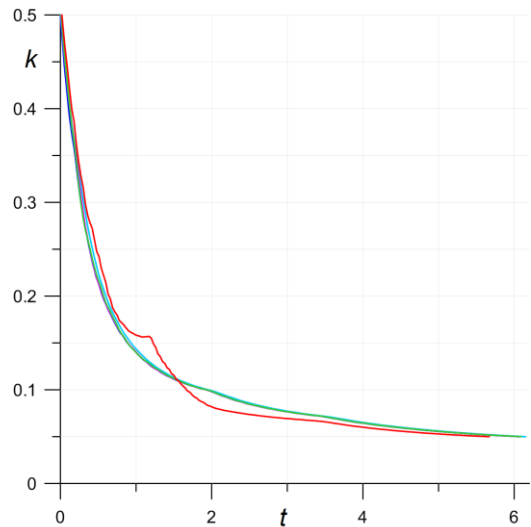


Fig. 7. Turbulent kinetic energy decay $k(t)/k_0$ in “ILES” $K = 1$, initial CFL = 2. Lines: blue – explicit time stepping, light-blue – DTS1, magenta – DTS2, green – DTS3, red – DTS4

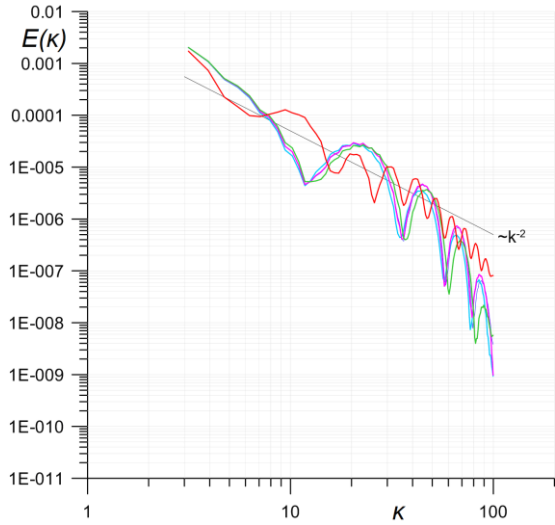


Fig. 8. Energy spectra $E(\kappa)$ in “ILES” $K = 1$, initial CFL = 2. Lines as in Fig. 7

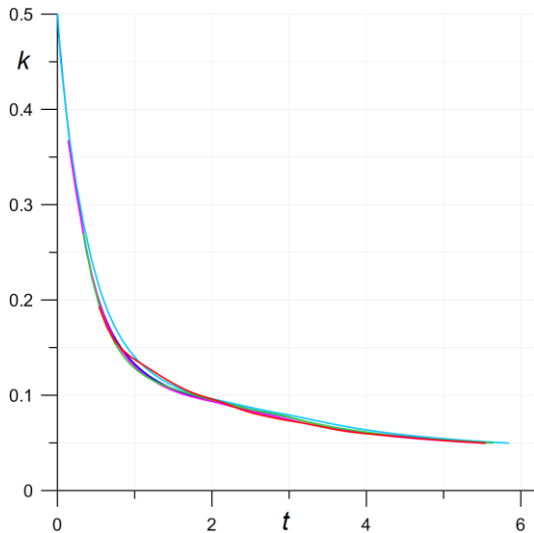


Fig. 9. Turbulent kinetic energy decay $k(t)/k_0$ in “LES” $K = 3$, initial CFL = 2. Lines as in Fig. 7

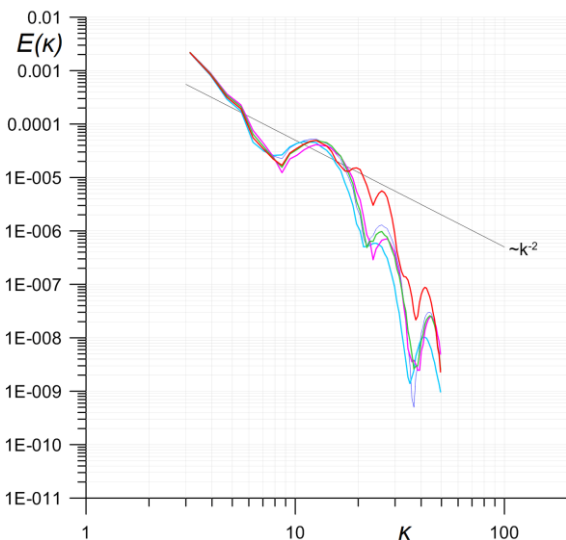


Fig. 10. Energy spectra $E(\kappa)$ in “LES” $K = 3$, initial CFL = 2. Lines as in Fig. 7.

All DTS schemes were found to be conditionally stable allowing time marching with CFL up to 1–4. The problem is assumed to be with DTS approximation of nonlinear convective fluxes. It looks like it is linearization procedure which makes conventional implicit schemes unconditionally stable. This finding makes the possibility of high CFL DTS computations questionable on highly stretched (e.g. boundary layer) meshes at least in low viscosity regions.

Higher order DTS schemes (DTS3, DTS4) are quite non-monotone and have lower limiting CFL value than lower order DTS schemes (DTS1, DTS2); this behavior is seen in the DTS4 plots obtained with initial CFL = 2: both $k(t)/k_0$ and $E(\kappa)$ are distorted relative to the other solutions.

With lower initial CFL = 0.5, the difference between different DTS schemes disappears; all the solutions are close to global time stepping solution.

To sum up, in the current test subgrid model only damps small scale motions and makes the solution smoother and simpler to converge; Smagorinsky model efficiently eliminates DG scheme non-monotonicity near the discontinuities and is recommended for use but with substantially lower C_s value.

2.6 Solutions comparison in terms of efficiency

No evident dependency of run time on DTS order was found in computations. Run times scale approximately inversely with CFL, see Fig. 11. $K = 3$ “LES” computation takes 1.34–1.80x more time than $K = 1$ “ILES” on the same NDOFs using dual time stepping and 1.83–1.89x more time than $K = 1$ “ILES” using explicit time stepping. Most importantly, explicit scheme is 9x **faster** than DTS schemes despite 67x lower time step. Therefore, according to 1D Burgers equation test, it is recommended to use explicit schemes for unsteady computations, at least when a mesh is close to uniform.

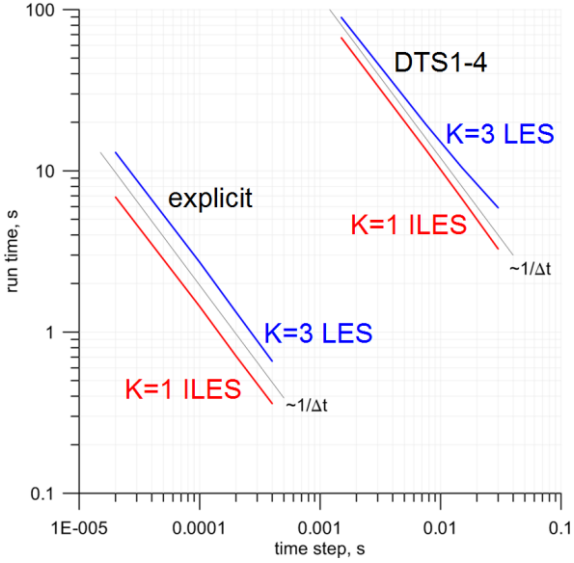


Fig. 11. Performance comparison: run time vs. time step, 1D Burgers equation test case

3 Three-dimensional isotropic turbulence test

3.1 Computational domain, initial and boundary conditions

A three-dimensional computational domain $[0, 2\pi] \times [0, 2\pi] \times [0, 2\pi]$ m with periodic boundary conditions is used in this test. Initial condition is a random velocity field $u_i(\mathbf{x}, 0)$ in the form of

$$u_i(\mathbf{x}, 0) = \sum_{n=1}^N \hat{u}_i(\mathbf{k}_n) \cos(\mathbf{k}_n \cdot \mathbf{x} + \varphi_n).$$

The value \hat{u}_i is randomly generated with the following properties:

$$\langle \hat{u}_i \rangle = 0; \langle \hat{u}_i \hat{u}_j \rangle = b_{ij} \Delta \mathbf{k} = \frac{E(k)}{4\pi k^2} \left(\delta_{ij} - \frac{k_i k_j}{k^2} \right) \Delta \mathbf{k}.$$

Here b_{ij} stands for correlation tensor of isotropic turbulence, $\Delta \mathbf{k}$ is a volume of cell in phase space. The energy spectrum is chosen to be consistent with equilibrium state $E(\kappa) \sim C \kappa^{-5/3}$. The practical coefficient C in energy formula is chosen to achieve field with turbulence intensity of 1 m/s. The static pressure field is set constant over the domain. Viscosity coefficient value is determined according to Sutherland's formula.

3.2 Computational meshes, models, and numerical scheme settings

Computations with Implicit large eddy simulation (ILES) and Large eddy simulation (LES) have been conducted.

ILES computations use mesh with $55 \times 55 \times 55$ cells and DG $K=1$ (6.7×10^5 DOFs). Time-stepping strategies tested are 1st order explicit global time stepping (RK4, a 4 step 4th order Runge-Kutta scheme) and 2nd order DTS1–DTS4.

LES computations use mesh with $32 \times 32 \times 32$ cells and DG $K=3$ (6.6×10^5 DOFs). The same time-stepping strategies tested: explicit global time stepping (RK4) and DTS1–DTS4. The subscale model is Smagorinsky with $C_S = 0.2$.

3.3 Results processing

Computations are performed until the turbulent kinetic energy value drops 10 times to its initial value k_0 . A typical velocity field is shown on Fig. 12.

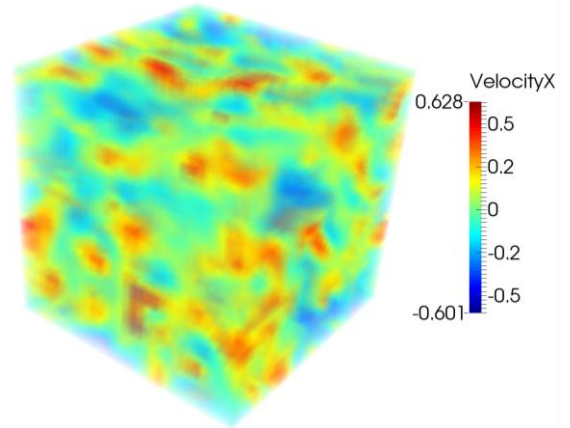


Fig. 12. A typical velocity field in three-dimensional isotropic turbulence test case

Turbulent kinetic energy is integrated over the whole computational domain using the same Gauss quadrature rules as in the rest of the numerical scheme. The dependence $k(t)$ on an interval from $k_0/2$ to $k_0/10$ is extracted and compared between computations.

Energy spectrum $E(\kappa)$ at the final moment of computation is determined and compared.

Integration is done over all cells utilizing discrete 3D Fourier transformation:

$$\hat{\mathbf{u}}(\mathbf{k}) = \frac{1}{2\pi^3} \iiint_0 \mathbf{u}(\mathbf{r}) \exp(-i\mathbf{k}\mathbf{r}) d\mathbf{r} .$$

The components of phase space vectors \mathbf{k} turn out to be integer for the chosen geometric domain. Then the energy spectrum is calculated as

$$E(\kappa) = \frac{1}{\Delta\kappa} \iiint_{\kappa-\Delta\kappa/2 < \mathbf{K} < \kappa+\Delta\kappa/2} 0.5\hat{\mathbf{u}}(\mathbf{K})\hat{\mathbf{u}}^*(\mathbf{K})d\mathbf{K}.$$

3.4 Solutions comparison in terms of accuracy

The accuracy of computations is controlled in two stages. The first is held during the computation and second is final control. In both stages the DTS solutions are compared to the references, which are explicit global time-step RK4. These references give us the dependency of turbulence kinetic energy on time $k(t)$ and turbulence energy spectrum $E(\kappa)$ at the final step of computation.

Energy spectra for successful $K=1$ ILES computations are shown in Fig. 13, for $K=3$ LES computations – in Fig. 14.

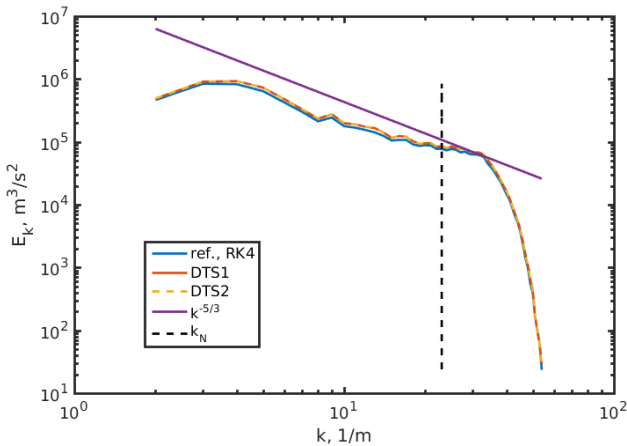


Fig. 13. Energy spectra $E(\kappa)$ in ILES $K=1$ computations. k_N stands for Nyquist wavenumber

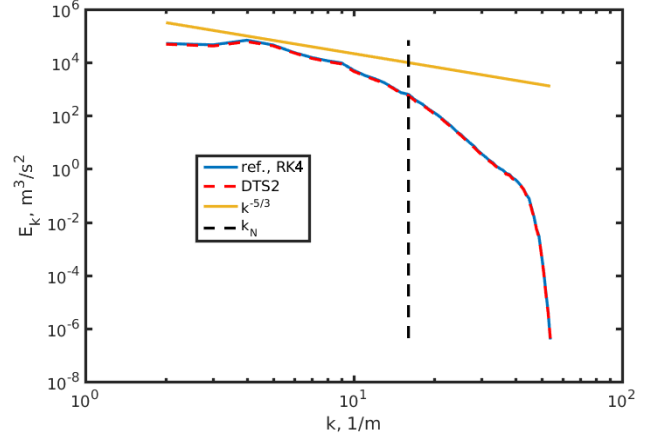


Fig. 14. Energy spectra $E(\kappa)$ in LES $K=3$ computations. k_N stands for Nyquist wavenumber

The DTS computations imply the large work on setting up optimal computation parameters. The question to choose optimal CFL, convergence depth for inner iterations, type of convergence (relative or absolute) is of the main concern.

DTS3 and DTS4 runs in general are failed. The main result is in unbounded oscillations growth. This corresponds to the Burgers equation test case where higher order DTS schemes appeared to distort the solutions. Tuning the parameters, yields suppressed growth of oscillations, but the accuracy remains very poor. Good accuracy for DTS3 was achieved with LES $K=3$, but the resulting speed of computation left no chance to finalize it in reasonable time.

All successful computations (explicit time stepping, DTS1, DTS2) produced almost identical results. The $K=3$ LES solution give highly damped energy spectrum, especially at medium and high wavenumbers. The $K=1$ ILES solution results in resolution of $\kappa^{-5/3}$ spectrum up to $\kappa \sim 20 \text{ m}^3/\text{s}^2$. This result again shows that standard $C_s = 0.2$ value is excessive and suggests trying Smagorinsky subgrid model with lower C_s or even $K=3$ ILES in the future.

3.5 Solutions comparison in terms of efficiency

Concerning the required memory, $K=1$ ILES computation used 2.2 Gb RAM while $K=3$ LES computation used 4.8 Gb RAM.

Run times (in CPU units) are collected in the following table:

time stepping	$K=1$ ILES	$K=3$ LES
global	3.56×10^4	11.6×10^4
DTS1	16.8×10^4	poor accuracy
DTS2	16.5×10^4	25.6×10^4

As in Burgers equation test, there is no evident dependency of run time on DTS order. $K=3$ LES computation takes 1.5–3.3x more time than $K=1$ ILES on the same NDOFs. Again, explicit scheme is 2.2–4.7x **faster** than DTS schemes despite much lower time step. Besides, DTS scheme requires additional time for optimal convergence criterion search to provide reliable quality of computation and acceptable efficiency.

Therefore, according to 3D isotropic turbulence test, it is recommended to use explicit schemes for unsteady computations, at least when a mesh is close to uniform.

3 Conclusions

Dual time stepping techniques for Discontinuous Galerkin method are presented for one-dimensional Burgers equation and for full three-dimensional Navier–Stokes equation system. The results of two test cases computations are reported which allow to make the following conclusions:

1. Smagorinsky subscale model used with DG $K=3$ is more dissipative than DG $K=1$ ILES on the same NDOF, although both models are able to capture some part of $E(\kappa)$ inertial subrange. It is proposed to try lower C_s values with high order DG schemes.

2. $K=1$ DG ILES is up to 3 times more efficient than DG $K=3$ LES with the same NDOF.

3. There is no difference in efficiency between DTS1–DTS4, but DTS3 and DTS4 solutions suffer from increased non-

monotonicity. DTS2 looks the best compromise among dual time stepping schemes considered.

4. Explicit scheme is several times faster than DTS despite significantly lower time steps. It is recommended to use explicit schemes for unsteady computations (at least when a mesh is close to uniform).

The work was supported by Russian Ministry of Education and Science within the Federal Target Program “Studies and Designs on Priority Directions of the Russian Science-Technology Complex Development in 2014-2020”, agreement No. 14.628.21.0005, unique project identifier: RFMEFI62815X0005.

References

- [1] Grinstein FF, Margolin LG and Rider WJ (eds). *Implicit large eddy simulation: Computing turbulent fluid dynamics*. Cambridge Univ. Press, 2007.
- [2] Smagorinsky J. General circulation experiments with the primitive equations. I. The basic experiment. *Mon. Weather Rev.*, Vol. 101, pp 99-164, 1963.
- [3] Venkateswaran S, Merkle CL. Dual time-stepping and preconditioning for unsteady computations. *Proc 33rd Aerospace Sciences Meeting and Exhibit*, Reno, NV, USA, 1995.
- [4] Bassi F, Botti L, Colombo A, Di Pietro DA and Tesini P. On the flexibility of agglomeration based physical space discontinuous Galerkin discretizations. *J. Comput. Physics*, Vol. 231, No. 1, pp 45-65, 2011.
- [5] Bassi F, Rebay F, Mariotti G, Pedinotti S and Savini M. A high-order accurate discontinuous finite element method for inviscid and viscous turbomachinery flows. *Proc 2nd European Conference on Turbomachinery – Fluid Dynamics and Thermodynamics*, Antwerpen, Belgium, pp 99-108, 1997.
- [6] Ortega JM. *Introduction to parallel and vector solution of linear systems*. Plenum Press, 1988.
- [7] Bosnyakov IS, Mikhaylov SV, Morozov AN, Podaruev VY, Troshin AI, Vlasenko VV, Wolkov AV, Garcia-Uceda A, Hirsch Ch. Implementation of high-order discontinuous Galerkin method for solution of practical tasks in external aerodynamics and aeroacoustics. In *IDIHOM: Industrialization of High-Order Methods – A Top-Down Approach*. Springer, 2015.

4 Contact Author Email Address

Contact author is Alexey Troshin, email: ai-troshin@yandex.ru

Copyright Statement

The authors confirm that they, and/or their company or organization, hold copyright on all of the original material included in this paper. The authors also confirm that they have obtained permission, from the copyright holder of any third party material included in this paper, to publish it as part of their paper. The authors confirm that they give permission, or have obtained permission from the copyright holder of this paper, for the publication and distribution of this paper as part of the ICAS proceedings or as individual off-prints from the proceedings.